The Pharma Innovation Journal 2023; SP-12(10): 721-732

www.ThePharmaJournal.com

The Pharma Innovation

ISSN (E): 2277-7695
ISSN (P): 2349-8242
NAAS Rating: 5.23
TPI 2023; SP-12(10): 721-732

www.thepharmajournal.com
Received: 01-07-2023
Accepted: 06-08-2023

Pratyush
Faculty, Department of Civil Engineering, Kamla Nehru Institute of Technology, Sultanpur, Uttar Pradesh, India

Corresponding Author:
Pratyush
Faculty, Department of Civil Engineering, Kamla Nehru Institute of Technology, Sultanpur, Uttar Pradesh, India

Investigation of seismic performance on retaining walls

Pratyush

Abstract
For the secure construction of the wall used for retaining purposes in earthquake-prone areas, the seismic effect of both active and passive pressures on the ground must be determined. The impact of waves caused by Rayleigh is not taken into account by pseudo-static and pseudo-dynamic approaches. About 67% of the entire energy from earthquakes is made up of Rayleigh waves. In the present study, the active as well as passive ground pressures are compared using a new pseudo-dynamic approach developed by Deepankar Chaudhary Amey Deepak Katdare. This most recent pseudo-dynamic technique takes into account waves produced by Rayleigh, waves caused by shear, and principal waves. The prerequisite of zero pressure on the earth's surface is accomplished by using this technique.

Keywords: Pseudo dynamic, zero ground stress Rayleigh waves, retaining wall, Mononobe-Okabe method

Introduction
The calculation based on the lateral static pressure of the earth on the structure of a retaining wall was made by Coulomb in 1776. When determining the size of the push on the retaining wall, Coulomb employed the equilibrium of forces to obtain the greatest state of passiveness and the least active mode criteria. As a result of the need to investigate a significant number of rupture surfaces in order to pinpoint the crucial failure plane, the challenge is unsolvable. In 1857, Rankine offered a straightforward technique for calculating the highest passive and lowest active ground stress. According to Rankine, the backfill soil experienced shear collapse. The assessment of static pressure on the ground and the construction of the retaining structure are both based on the methods presented by Coulomb and Rankine.

For several decades, masonry construction has been a common structural type used all over the world. In China, buildings made of masonry are still seen as the best choice for rural construction, despite buildings made of reinforced concrete having recently taken over urban development due to their quick construction times. This is because materials for masonry are straightforward and affordable. However, it was found that masonry constructions had poor seismic resilience, and in the earthquake that struck Wenchuan, 74% of all brick masonry buildings fell or suffered significant damage [1]. Therefore, it has become a focus of study to enhance the seismic behaviour of masonry constructions in rural areas.

In order to enhance the seismic endurance of buildings made of masonry, several studies, both theoretical and experimental, have been conducted on different components of these structures. On the one hand, investigation into novel structural forms has been done. The impact of the horizontal reinforcement on the earthquake resistance of the specimens was investigated using cyclic tests by Haach *et al.* [2] as shown in figure (1), who developed a novel horizontal trussed reinforcement for concrete-reinforcement walls made from masonry. The findings emphasised that the existence of horizontal reinforcement provides superior fracture control and dispersion. The earthquake resistance of ten single-story buildings constructed with reinforced concrete walls made of masonry was examined by Voon and Ingham [3], along with the impact of imposed axial compressive stresses and shear reinforcement. The outcomes demonstrated that the specimens' shear strength increased the magnitude of the imposed axial stress that was observed. Eldin *et al.* [4–7], Obaidat *et al.* [8], Bolhassani *et al.* [9–11], Ramirez *et al.* [10–11], and EI-Dakhakhni *et al.* [12] have all performed studies on the seismic behaviour of concrete with reinforcement walls made from masonry. Additionally, periodic load assessment was done when Ma *et al.* [13] built a shear wall using a unique sort of core-aligned block called a double H-block. According to the findings, the double H-block masonry shear barrier had a high degree of ductility and dissipation of energy. Four unconstrained posttensioned walls of masonry were the subject of an experimental investigation conducted by Hassanili *et al.* [14, 15].

The findings demonstrate that, for a given total starting posttensioned force, the distribution of posttensioned bars affects the specimen's lateral toughness. The unconstrained post-tensioning examples resemble swaying walls, and analogous and pertinent research has also been done by Ryu *et al*. [16], Wight *et al*. [17], Kalliontzis and Schultz [18], and Roseboom and Kowalsky [19].

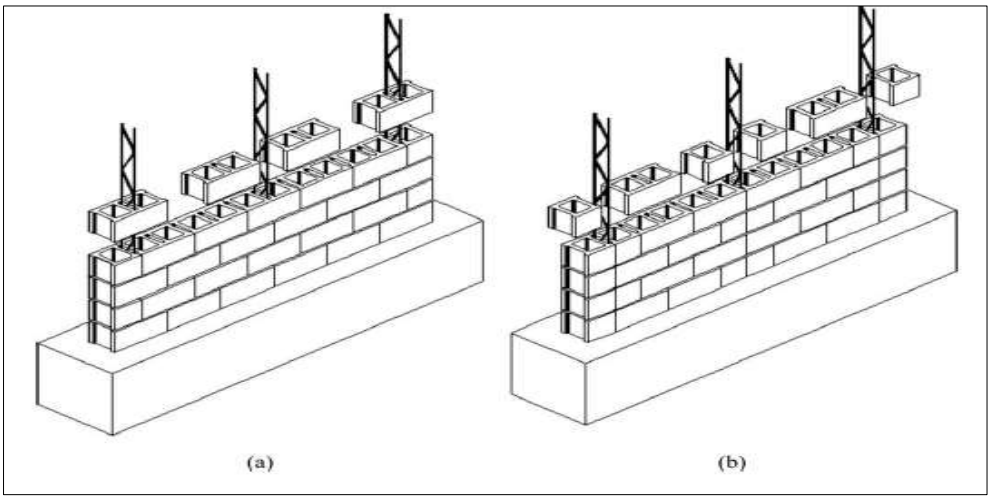

Fig 1: The masonry bond patterns

Mononobe Okabe Method

Mahmoud *et al*. [20], a preliminary approach to calculating the combination of static as well as dynamic pressures of the earth on wall-retaining structures was suggested. This enhanced version of the Coulomb sliding wedge concept, which has its foundation on the plasticity concept, represents the forces of earthquakes by corresponding static force. The technique was created for dry, cohesion-free soil.

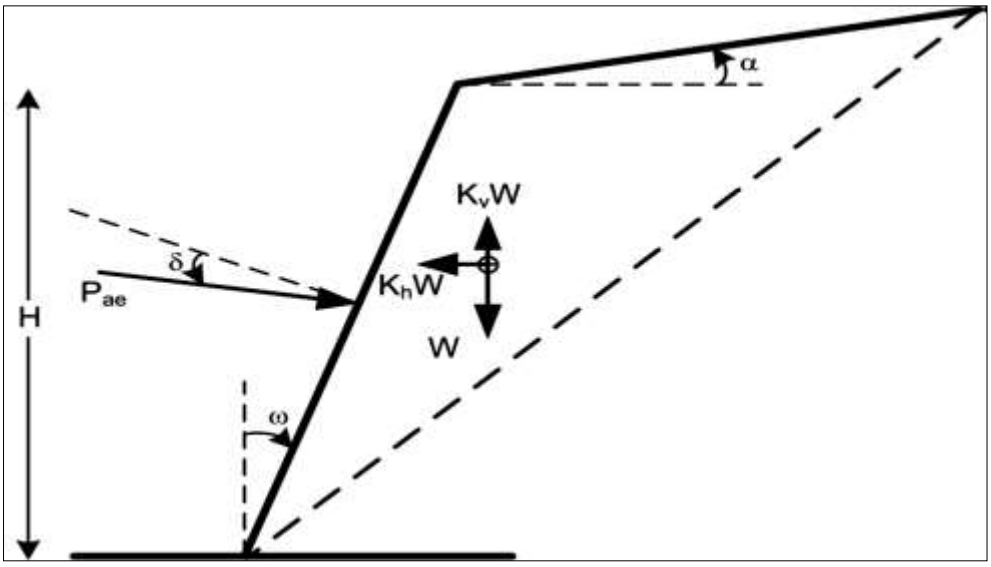

Fig 2: The stresses on the soil wedge

The wedge's active force is calculated as:

$$P_{AE} = \frac{1}{2} \gamma H^2 (1- k_V) K_{AE} \quad (1)$$

$$K_{AE} = \frac{cos2(\phi-\theta-\beta)}{cos\theta cos2\beta \cos(\delta+\beta+\theta)[1+\sqrt{\frac{\sin(\phi+\delta)\sin(\phi-\theta-i)}{\cos(\delta+\beta+\theta)\cos(i-\beta)}}]2} \quad (2)$$

$$\theta = \tan\text{-}1(\frac{kh}{1-kv}) \quad (3)$$

The Mononobe-Okabe active pressure on the earth formula is represented by equation (1).

The passive force P_{PE} is calculated as:

$$P_{PE} = \frac{1}{2} \gamma H^2 (1- k_V) K_{PE} \quad (4)$$

$$K_{PE} = \frac{cos2(\phi-\theta+\beta)}{cos\theta cos2\beta \cos(\delta-\beta+\theta)[1-\sqrt{\frac{\sin(\phi+\delta)\sin(\phi+\theta-i)}{\cos(\delta-\beta+\theta)\cos(i-\beta)}}]2} \quad (5)$$

Where

$\theta = \tan\text{-}1 (\frac{kh}{1-kv})$

H: Height of wall
i: Slope of backfill
K_{AE}: Active earth pressure coefficient
P_{AE}: Active force per unit length of wall
P_{Pe}: Passive force per unit length of wall
B: Slope of back of the wall with respect to vertical
Δ: Angle of friction between wall and soil
Y: Unit weight of soil
Φ: Soil friction angle

Pseudo-dynamic method

The examination takes an upward, stiff wall of retention into account. This approach takes into account all varieties of seismic waves, including Rayleigh, shear, and main waves. The material used as the backfill beneath the wall that retains soil is thought to have less cohesiveness. Shear stresses and primary wave velocities (Vs and Vp) under earthquake circumstances are depicted in the figure. The shear modulus of the soil (G), the density of the soil (ρ), and the Poisson's ratio of the soil (ν) are all functions of the seismic wave velocities, and the Rayleigh velocity of the wave is a function of KR, where KR is the Rayleigh wave's wave number.

As seen in the image, a thin element with width dx and thickness dz is located at a distance of x from the surface of the wall.

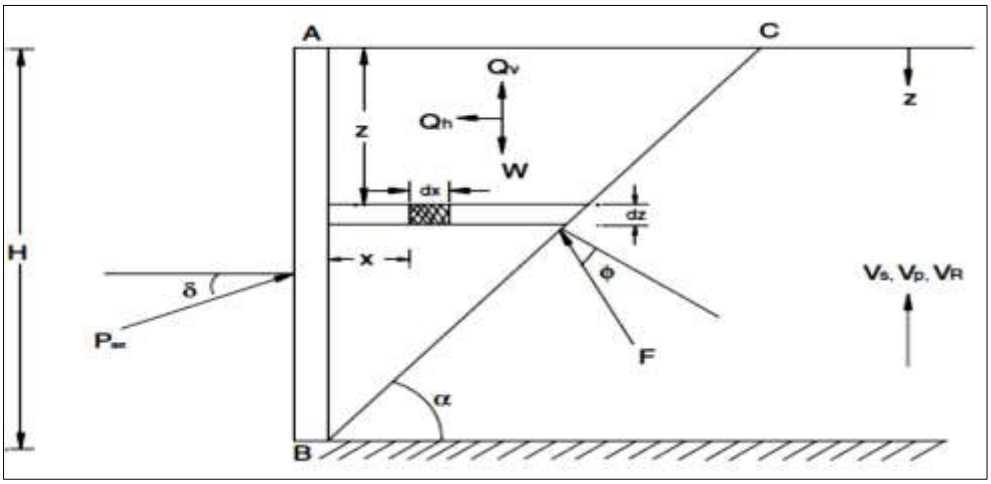

Fig 3: When calculating the active pressure of the earth, an upward retaining structure is taken into account.

Through the assistance of the boundary equilibrium strategy, the forces acting on the wedge are resolved, and the predicted total (static and dynamic) active pressure on the earth is displayed as,

$$P_{ae}(t) = \frac{Wsin(\alpha-\varphi) \pm Q_h \cos(\alpha-\varphi) \pm Q_v \sin(\alpha-\varphi)}{cos(\delta+\varphi-\alpha)} \quad (6)$$

The seismic active earth pressure coefficient (K_{ae}) is defined as,

$$K_{ae} = \frac{2P_{ae}(t)}{\gamma H^2} \quad (7)$$

$$K_{ae} = \frac{1}{\tan\alpha} \frac{\sin(\alpha-\varphi)}{\cos(\delta+\varphi-\alpha)}$$

$$-\left\{Q_h \left\{\frac{\gamma k_h}{(-K_R)g\tan\alpha} \frac{\sin\left(\omega t+\frac{K_R H}{\tan\alpha}\right)-\cos\omega t}{\sin(\omega t-K_R x)\left(e^{-qH}+\frac{2qs}{(S^2+K_R^2)q^2}e^{-sH}\right)}\left[\frac{2qe^{-qH}}{q^2}-\frac{2qK_R e^{-sH}}{(S^2+K_R^2)(s)}\right]\right\}\frac{\cos(\alpha-\varphi)}{\cos(\delta+\varphi-\alpha)}\right\}+$$

$$\left\{\frac{(2)k_v}{(-K_R)\tan\alpha}\frac{\cos\left(\omega t+\frac{K_R H}{\tan\alpha}\right)-\sin\omega t}{\cos(\omega t-K_R x)}\frac{\left[\frac{2qK_R^2e^{-qH}}{(s^2+K_R^2)q^2}-\frac{e^{-qH}}{qK_R}\right]}{\left[\frac{2qK_R}{(s^2+K_R^2)q^2}-\frac{qe^{-qH}}{K_R}\right]}\frac{\sin(\alpha-\varphi)}{\cos(\delta+\varphi-\alpha)}\right\} \quad (8)$$

By comparing the overall earthquake active resistance that is operating on the wall that is retaining it with regard to the wall's depth, it is possible to determine the amount of seismic active earth's pressure dispersion.

$$p_{ae}=\frac{dp_{ae}(t)}{dz}=\frac{\gamma z}{\tan\alpha}\frac{\sin(\alpha-\varphi)}{\cos(\delta+\varphi-\alpha)}$$

$$+\left\{\frac{a_h\gamma z}{g(-K_R)\tan\alpha}\frac{\cos\left(\omega t+\frac{K_R z}{\tan\alpha}\right)-\cos\omega t}{\sin(\omega t-K_R x)\left(e^{-qz}+\frac{2qs}{(s^2+K_R^2)q^2}e^{-sz}\right)(q)}\frac{\cos(\alpha-\varphi)}{\cos(\delta+\varphi-\alpha)}\right\}-\left\{\frac{a_v\gamma z}{g(-K_R)\tan\alpha}\frac{\sin\left(\omega t+\frac{K_R H}{\tan\alpha}\right)-\cos\omega t}{\sin(\omega t-K_R x)}\frac{\left[\frac{2qK_R^2e^{-qz}}{(s^2+K_R^2)q^2}-\frac{e^{-qz}}{qK_R}\right]}{\left[\frac{2qK_R}{(s^2+K_R^2)q^2}-\frac{qe^{-qz}}{K_R}\right]}\frac{\sin(\alpha-\varphi)}{\cos(\delta+\varphi-\alpha)}\right\} \quad (9)$$

Condition of Passive Resistance

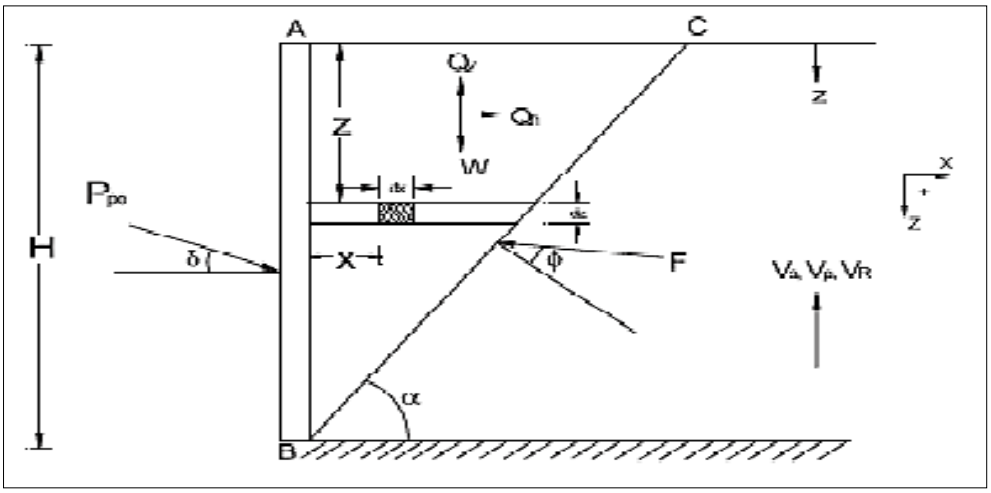

Fig 4: Calculating the active pressure of the earth, an upward wall of retaining is taken into account.

Assume a fixed-base vertically cantilever structure AB with a height H that supports a horizontal backfill with minimal cohesiveness, as shown in Fig. a piece that is dz in thickness at z distances from the highest point of the wall that is retaining and dx in width at x distances.

Overall passive resistance (static and dynamic) is calculated by applying the limit state of equilibrium technique to the forces acting against the wedge.

$$P_{pe}(t)=\frac{W\sin(\alpha+\phi)\pm Q_h\cos(\alpha+\phi)\pm Q_v\sin(\alpha+\phi)}{\cos(\alpha+\delta+\phi)} \quad (10)$$

The seismic passive earth pressure coefficient (K_{pe}) is given as

$$K_{pe}=\frac{2p_{pe}(t)}{\gamma H^2} \quad (11)$$

$$K_{pe}=\frac{1}{\tan\alpha}\frac{\sin(\alpha+\phi)}{\cos(\alpha+\delta+\phi)}-\left\{\frac{2a_h}{g\gamma H^2(-K_R)\tan\alpha}\frac{\cos\left[\omega t-K_R\left(\frac{H}{\tan\alpha}\right)\right]}{\sin(\omega t-K_R(x))\left[e^{-qz}+\frac{2qs}{[s^2+K_R^2]q^2}e^{-sz}\right]}\left[\frac{2qe^{-qH}}{q^2}-\frac{2qK_Re^{-sH}}{[s^2+K_R^2](s)}\right]\frac{\cos(\alpha+\phi)}{\cos(\alpha+\delta+\phi)}\right\}+$$

$$\frac{2a_v}{g(-K_R)\gamma H^2(K_R)\tan\alpha}\frac{\sin\left[\omega t-K_R\left(\frac{H}{\tan\alpha}\right)\right]}{\cos(\omega t-K_R(x))}\frac{\left[\frac{2q(K_R)e^{-sz}}{[s^2+K_R^2](-s)}-\frac{e^{-qz}}{q}\right]}{\left[\frac{2qK_R}{[s^2+K_R^2]q^2}-\frac{qe^{-qz}}{K_R}\right]}\frac{\sin(\alpha+\phi)}{\cos(\alpha+\delta+\phi)} \quad (12)$$

The distribution of the seismic passive earth pressure (p_{pe}) is given by

$$p_{pe}(t)=\frac{dp_{pe}(t)}{dz}==\frac{\gamma z}{\tan\alpha}\frac{\sin(\alpha-\phi)}{\cos(\alpha+\delta+\phi)}+\left\{\frac{a_h\gamma z}{g(-K_R)\tan\alpha}\frac{\cos[\omega t-K_R(x)]}{\sin(\omega t-K_R(x))(e^{-qz}+Be^{-sz})(qz)}\frac{\cos(\alpha-\phi)}{\cos(\alpha+\delta+\phi)}\left[\frac{2qe^{-qH}}{q^2}-\frac{2qK_Re^{-sH}}{[s^2+K_R^2](s)}\right]\right\}-$$

$$\frac{a_v\gamma z}{g(-K_R)\tan\alpha}\frac{\sin[\omega t-K_R(x)]}{\cos(\omega t-K_R(x))}\frac{\left[\frac{2q(K_R)e^{-sz}}{[s^2+K_R^2](-s)}-\frac{e^{-qz}}{q}\right]}{\left[\frac{2qK_R}{[s^2+K_R^2]q^2}-\frac{qe^{-qz}}{K_R}\right]}\frac{\sin(\alpha-\phi)}{\cos(\alpha+\delta-\phi)} \quad (13)$$

Where,

g	Acceleration due to gravity;
H	Height of retaining wall;
K_{pe}	Seismic passive earth pressure coefficient;
K_R	Wave number for Rayleigh wave;
k	Seismic acceleration coefficient;
k_h, k_v	Seismic acceleration coefficient in horizontal and vertical directions, respectively;
P_{pe}	Dynamic passive resistance;

$$q = \sqrt{K_R^2 - \left(\frac{\omega^2}{V_p^2}\right)}$$

$$s = \sqrt{K_R^2 - \left(\frac{\omega^2}{V_s^2}\right)}$$

T	Period of lateral shaking;
t	Time;
V_p	Primary wave velocity;
V_R	Rayleigh wave velocity;
V_s	Shear wave velocity;
α	Angle of inclination of failure surface to the horizontal;
γ	Unit weight of soil;
δ	Wall friction angle;
ϕ	Soil friction angle; and
ω	Angular frequency of base shaking.

Results and Discussions

Shear wave velocity, V_s =80 m/s, ratio of primary and shear wave velocity, V_p/V_S =1.87 and ratio of Rayleigh and primary wave velocity, $V_R/V_p = \alpha K_{Rs}$,

Where

$\alpha = \sqrt{(1-2\upsilon)/(2-2\upsilon)}$ and $K_{Rs}^6 - 8K_{Rs}^4 + (24\text{-}16\propto^2)\, K_{Rs}^2 + 16(\propto^2 - 1) = 0$ with $K_{Rs} = \frac{V_R}{V_s}$;

Unit weight of soil: γ 16 KN/m^3;
Height of wall: H: 5 m;
Poisson's ratio of soil: ν 0.3

K_{pe} variation with the failure plane (α)

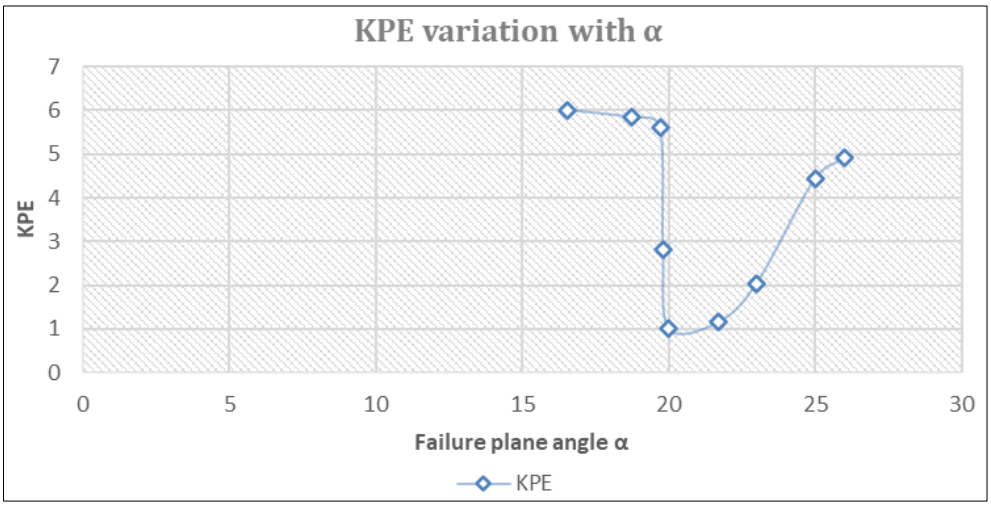

Fig 5: KPE variation with α

The point of failure plane is defined as 20. The valve for Kpe decreases as the failure plane angle increases, reaching its lowest at 20 before beginning to increase once more.

Soil Friction Angle's Effect on P_{pe}

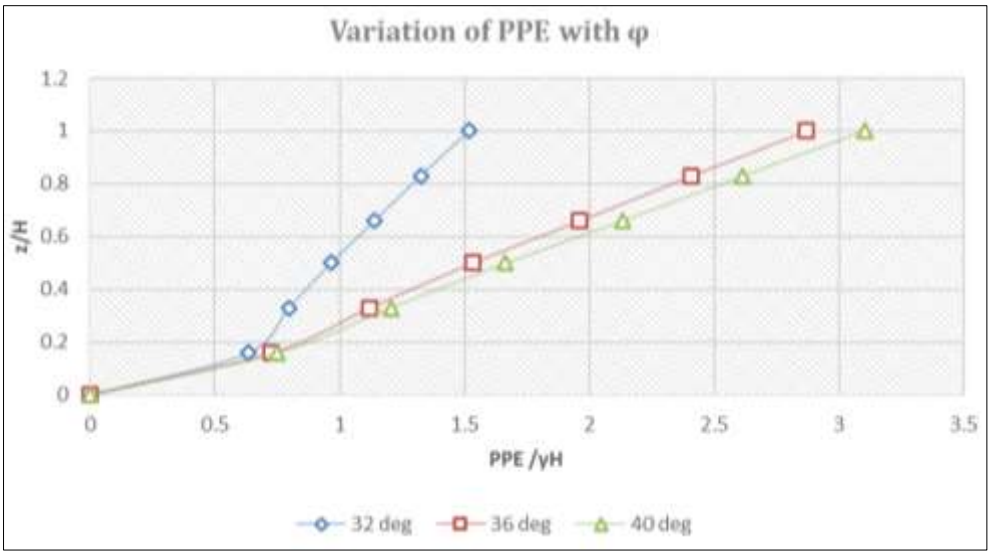

Fig 6: Variation of PPE

The passive pressure of the earth throughout the height of the structure rises as the soil angle of friction rises from 32° to 40°, and it is discovered to be at its highest for a soil friction angle of 40°. As the soil angle of friction rises from 36 to 40 degrees at a height ratio of z/H =1, passive pressure increases by roughly 8.14%.

Effect of K_h and K_v on the K_{pe}

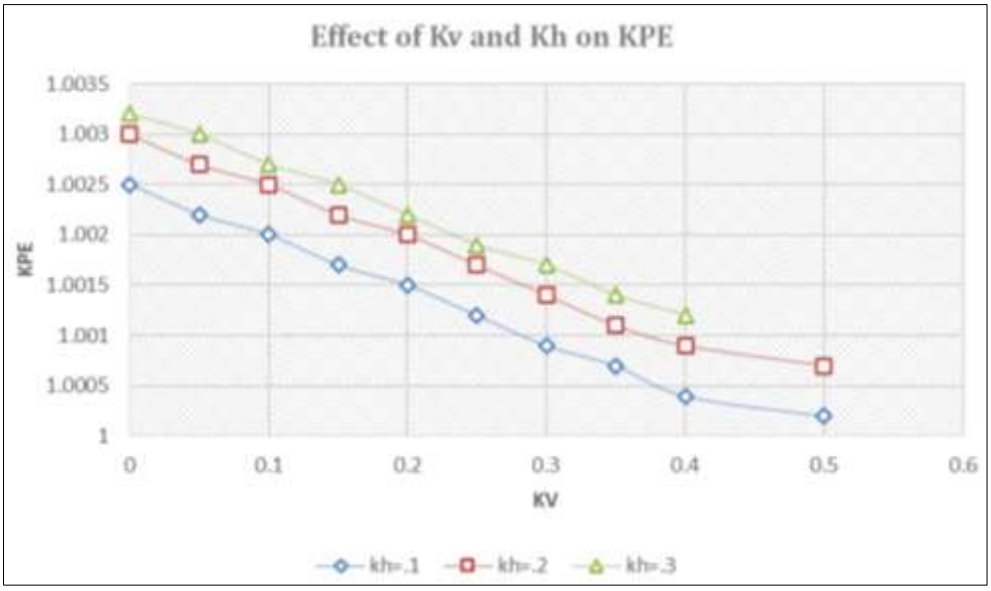

Fig 7: Effect of Kv and Kh on KPE

The Kpe valve improves with a rise in the earthquake horizontal coefficient valve, while Kpe decreases with a rise in the earthquake vertical coefficient valve.

Effect of the Rayleigh wave velocity on K_{pe}

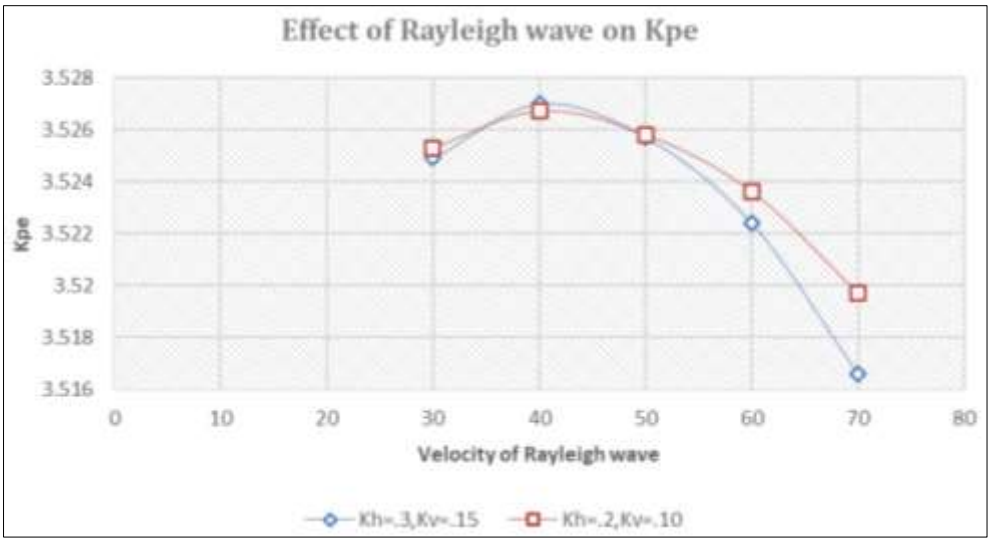

Fig 8: Effect of the Rayleigh wave on Kpe

The Kpe valve decreases as the Rayleigh velocity of the wave rises, reaching a maximum at 40 m/s.

Effect of failure plane on K_{ae}

Soil friction angle (α): 32˚
t/T: 0.03

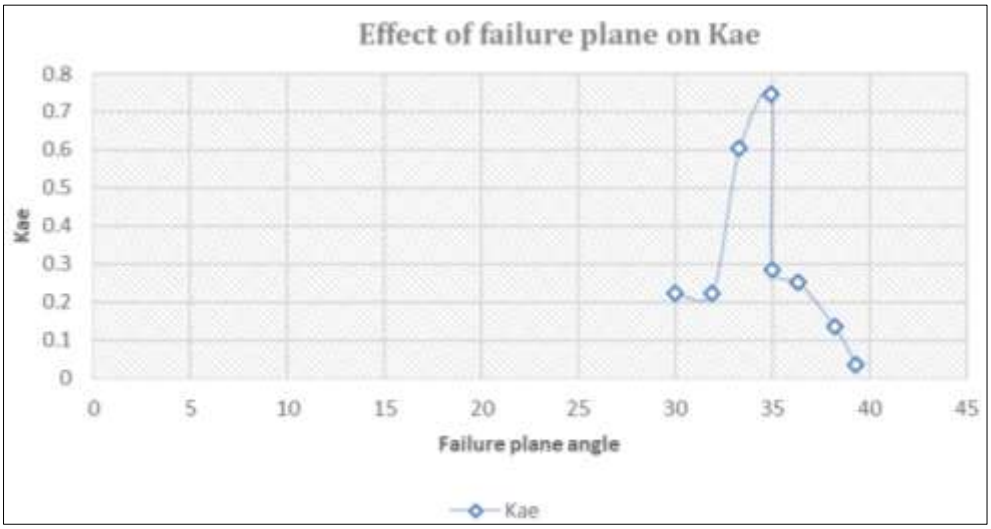

Fig 9: Effect of failure plane on Kae

The Kae valve grows along with the failure plane angle and achieves its maximum at 34.9. The Kae valve then closes less.

Effect of soil friction angle on the seismic active pressure P_{ae}

The flow through the distribution valve for seismically active pressure decreases as the soil internal friction angle increases. If the soil angle of friction is increased from 32 to 40 at z/H = 1, there is a drop of 4.20% in the $P_{ae}/\gamma H$ valve.

Effect of Rayleigh wave velocity on K_{ae}

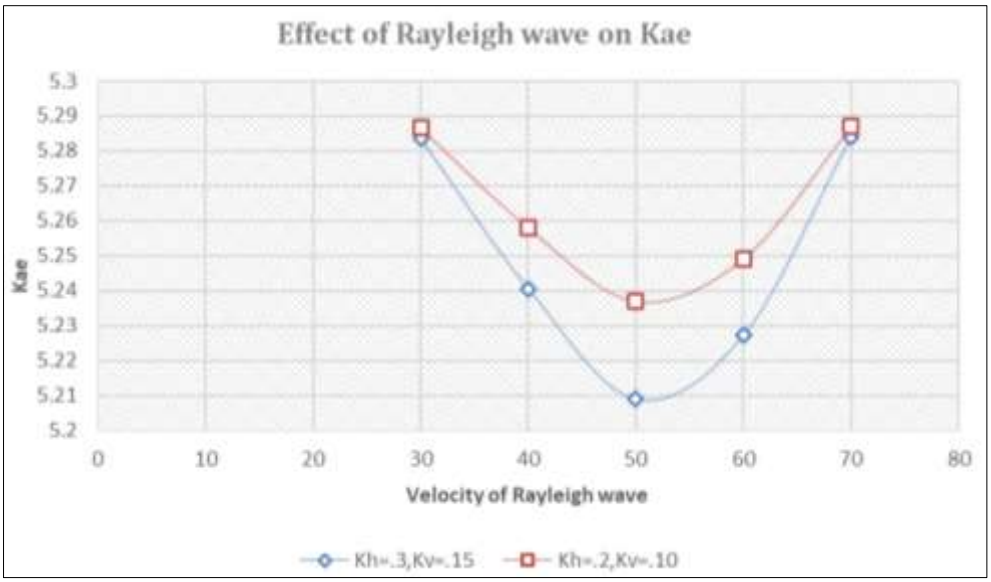

Fig 10: Effect of Rayleigh wave on Kae

The valve of Kae decreases and approaches a minimum speed of 50 m/s as the Rayleigh wave velocity rises. The Kae valve is then enlarged as the velocity rises.

Comparison of Seismic passive pressure by Mononobe–Okabe and Deepankar Chaudhury (new method)
Soil friction angle: 32˚
Wall friction angle: ϕ/2
K_h: 0.2
K_v: 0.5 K_h
t/T: 0.40

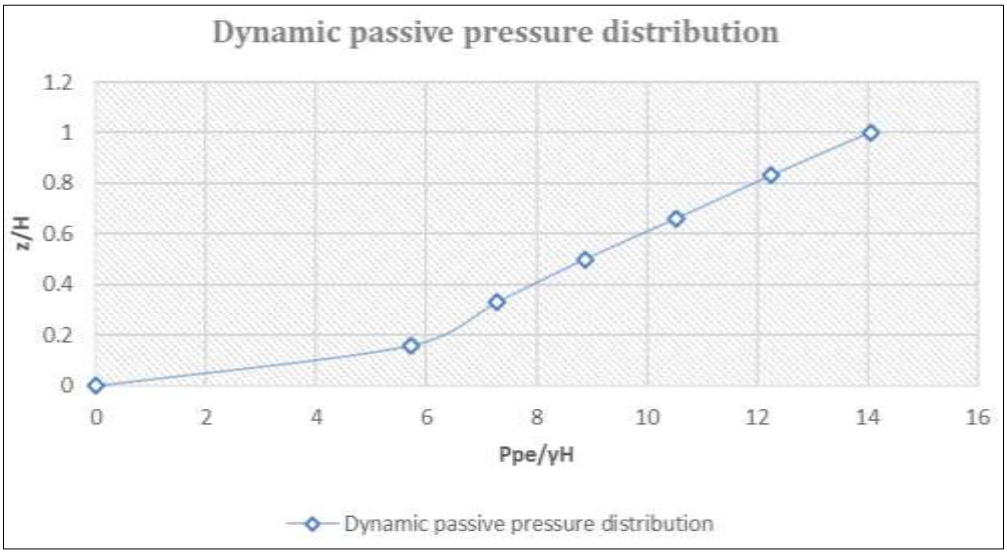

Fig 11: Dynamic passive pressure distribution

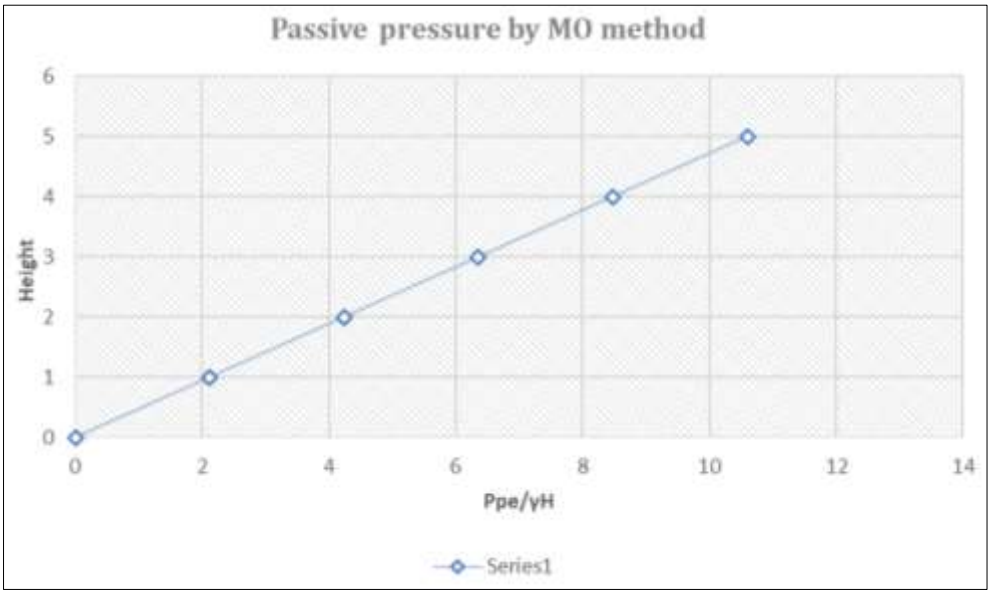

Fig 12: Passive pressure by M0 method

When the elevation of the wall used for retaining is compared to the earthquake passive pressure using the new technique and the Mononobe-Okabe method, it is discovered that the pressure has increased by 10.56%.

Comparison of seismic active pressure by MO and Deepankar Chaudhury (New method)
Soil friction angle: 32˚
Wall friction angle: ϕ/2
K_h: 0.2
K_v : 0.5 K_h
t/T: 0.40
K_{ae}: 0.449

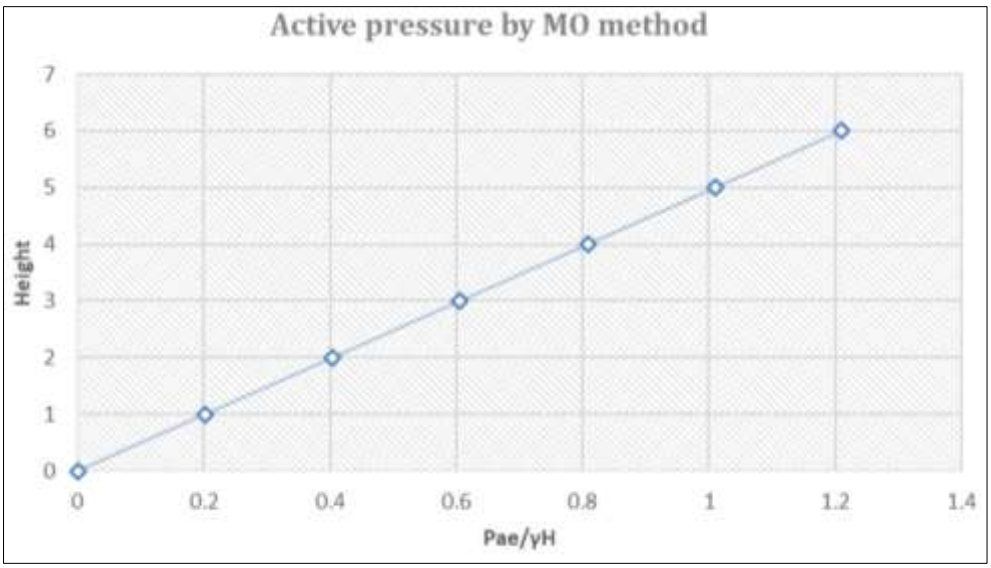

Fig 13: Active pressure by M0 method

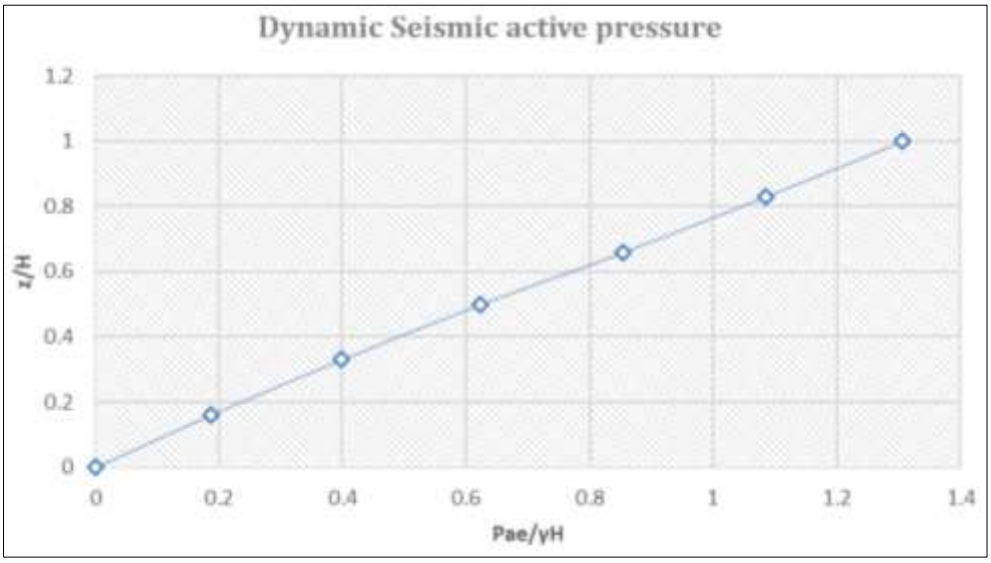

Fig 14: Dynamic Seismic active pressure

The earthquake's active pressure rises as the retaining wall's height increases. The pressure has increased by 7.97% when compared to the new method and the MO method.

Comparison of K_{ae} by Both Methods
Soil friction angle: 32 ˚
Wall friction angle: ϕ/2
K_h: 0, 0.1, 0.2, 0.3

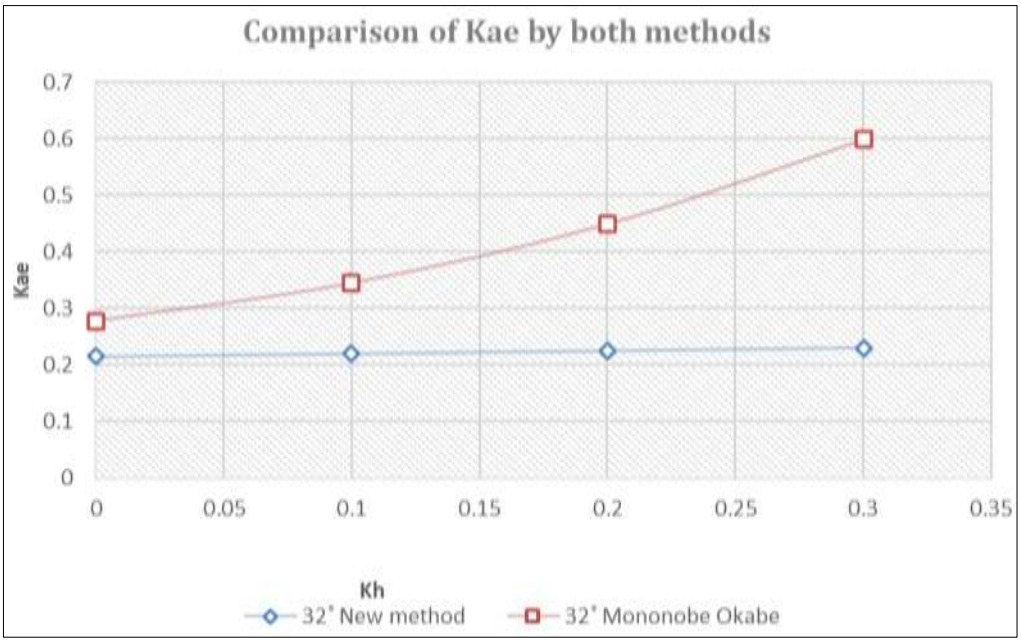

Fig 15: Comparison of Kae by both Methods

In all methods, the valve for Kae also grows when the valve for Kh increases. In comparison to the MO approach, the Kae valve has decreased by 61.18% using the new way.

Comparison of K_{pe} by Both Methods
Soil friction angle: 36 ˚
Wall friction angle: ϕ/2
K_h: 0, 0.1, 0.2, 0.3

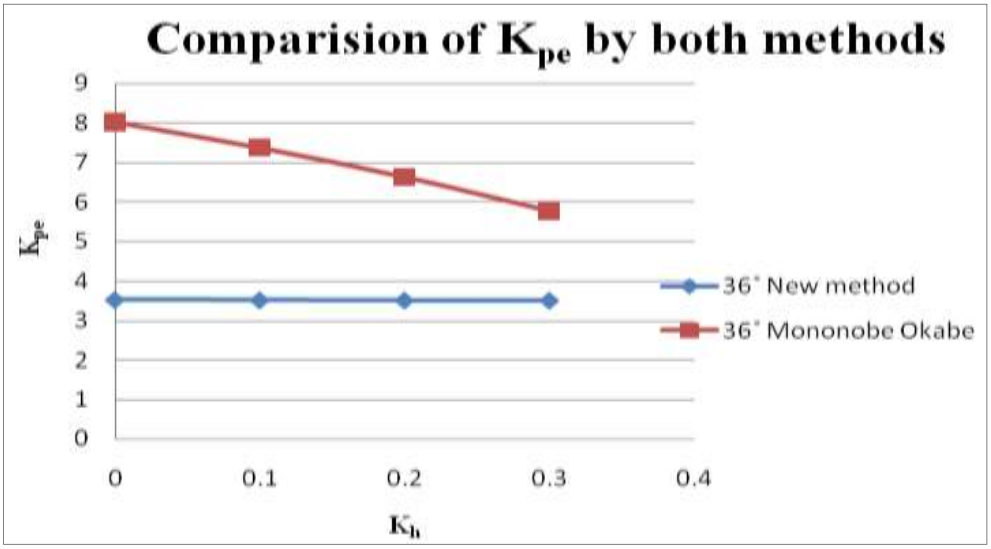

Fig 16: Comparison of Kae by both Methods

In all approaches, Kpe drops as the valve of Kh rises. The KPE valve has decreased by 49.24% in the new approach compared to the MO method.

Conclusions

Deepankar Chaudhury's (new pseudo-dynamic) technique takes into account all waves, including those generated by Rayleigh and principal waves. The Mononobe-Okabe approach is employed for the pseudo-static analysis. There is a rise of 7.97% when comparing earthquake active pressure using the new method with the Mononobe-Okabe approach. There is an increase of 10.56% when comparing the new approach to the MO method for passive pressure. When comparing the two methods, the Kae valve has a drop of 61.18%. The KPE disparity is 49.24%. The addition of the Rayleigh wave effect accounts for the differences between different valves. Therefore, it is essential to consider Rayleigh waves when analysing retaining walls.

References

1. Wang G, Li Y, Zheng N, Ingham JM. Testing and modelling the in-plane seismic response of clay brick masonry walls with boundary columns made of precast concrete interlocking blocks. Eng. Struct. 2017;131:513–529.
2. Haach VG, Vasconcelos G, Lourenco PB. Experimental Analysis of Reinforced Concrete Block Masonry Walls Subjected to In-Plane Cyclic Loading. J. Struct. Eng. 2010;136:452–462.
3. Voon KC. Ingham, J.M. Experimental In-Plane Shear Strength Investigation of Reinforced Concrete Masonry Walls. J. Struct. Eng. 2006;132:400–408.
4. Seif EIDin HM, Galal K. In-Plane Seismic Performance of Fully Grouted Reinforced Masonry Shear Walls. J. Struct. Eng. 2017;147:04017054.
5. Seif ElDin HM, Galal K. Effect of reinforcement anchorage end detail and spacing on seismic performance of masonry shear walls. Eng. Struct. 2018;157:268–279.
6. Seif ElDin HM, Aly N, Galal K. In-plane shear strength equation for fully grouted reinforced masonry shear walls. Eng. Struct. 2019;190:319-332.
7. Seif ElDin HM, Ashour A, Galal K. Seismic performance parameters of fully grouted reinforced masonry squat shear walls. Eng. Struct. 2019;187:518-527.
8. Obaidat AT, Ashour A, Galal K. Stress-Strain Behavior of C-Shaped Confined Concrete Masonry Boundary Elements of Reinforced Masonry Shear Walls. J. Struct. Eng. 2018;144:04018119.
9. Bolhassani M, Hamid AA, Johnson C, Moon FL, Schultz AE. New Design Detail to Enhance the Seismic Performance of Ordinary Reinforced Partially Grouted Masonry Structures. J. Struct. Eng. 2016;142:04016142.
10. Ramirez P, Sandoval C, Almazan JL. Experimental study on in-plane cyclic response of partially grouted reinforced concrete masonry shear walls. Eng. Struct. 2016;126:598–617.
11. Seif EIDin HM, Galal K. In-Plane Seismic Performance of Fully Grouted Reinforced Masonry Shear Walls. J. Struct. Eng. 2017;147:04017054.
12. EI-Dakhakhni WW, Banting BR, Miller SC. Seismic Performance Parameter Quantification of Shear-Critical Reinforced Concrete Masonry Squat Walls. J. Struct. Eng. 2013;139:957–973.
13. Ma G, Huang L, Yan L, Kasal B, Chen L, Tao C. Experimental performance of reinforced double H-block masonry shear walls under cyclic loading. Mater. Struct. 2017;50:70.
14. Hassanli R, EIgawady MA, Mills JE. Experimental Investigation of In-Plane Cyclic Response of Unbonded Posttensioned Masonry Walls. J. Struct. Eng. 2016;142:04015171.
15. Hassanli R, ElGawady MA, Mills JE. Simplified approach to predict the flexural strength of self-centering masonry walls. Eng. Struct. 2017;142:255-271.
16. Ryu D, Wijeyewickrema AC, EIGawady MA, Madurapperuma MAKM. Effects of Tendon Spacing on In-Plane Behavior of Posttensioned Masonry Walls. J. Struct. Eng. 2014;140:04013096.

17. Wight GD, Kowalsky MJ, Ingham JM. Shake table testing of posttensioned concrete masonry walls with openings. J. Struct. Eng. 2007;133:1551-1560.
18. Kalliontzis D, Schultz AE. Characterizing the In-Plane Rocking Response of Masonry Walls with Unbonded Posttensioning. J. Struct. Eng. 2017;143:04017110
19. Rosenboom OA, Kowalsky MJ. Reversed in-plane cyclic behavior of posttensioned clay brick masonry walls. J. Struct. Eng. 2004;130:787-798.
20. Mahmoud Yazdani, Ali Azad, Abol Hasan Farshi, Siamak Talatahari. Extended Mononobe-Okabe Method for Seismic Design of Retaining Walls, Journal of Applied Mathematics, vol. 2013, Article ID 136132, 10 pages, 2013. https://doi.org/10.1155/2013/136132